DOI:10.11835/j.issn.2096-6717.2020.089 开放科学(资源服务)标识码(OSID):

# Effect of the porosity the upstream building on the natural ventilation of the downstream building and the reliability of its computational fluid dynamics simulation

*FU Linli*[1], *YIN Wei*[1,2], *WANG Tianwen*[1], *ZHANG Guoqiang*[2]

(1. School of Civil Engineering; Hunan Engineering Research Center for Intelligently Prefabricated Passive House, Hunan University of Science and Technology, Xiangtan 411201, Hunan, P. R. China; 2. School of Architecture, Hunan University, Changsha 410007, P. R. China)

**Abstract**: Natural ventilation can reduce the concentration of indoor pollutants, including that of biological aerosols. It does this mainly by cross ventilation. However, in closely built-up cities, the shielding effect between buildings will significantly reduce the ventilation effect. Previous studies rarely considered the effects of a building's characteristics on other buildings. This preliminary study takes two buildings and investigates the influence of the position and size of nine different windows on their cross ventilation potential. It focuses on only one direction of incoming flow where the distance between the two buildings is two times the width of the building, first, analyzing the reliability of the computational fluid dynamics (CFD) simulation based on steady Reynolds-Averaged Navier-Stokes equations. The results reveal that the reliability of the computational fluid dynamics simulation in some cases is insufficient and that with a simulation of 20% porosity it is difficult to reproduce the wind pressure on a downstream building by computational fluid dynamics in comparison to 10% or 5% porosity. The different simulation reliability may be caused by the instability of the airflow between the buildings. However, using data from the wind tunnel, we found that the cross ventilation potential of the downstream building decreases with the increase of the window area of the upstream building, which is contrary to general beliefs.

**Keywords**: natural ventilation; cross ventilation; building shielding effects; CFD reliability; wind tunnel

# 上游建筑孔洞特性对下游建筑自然通风潜力的影响及其 CFD 模拟可靠性

付琳莉[1],殷维[1,2],王天文[1],张国强[2]

(1.湖南科技大学 土木工程学院;湖南省智慧建造装配式被动房工程技术研究中心,湖南 湘潭 411201;
2.湖南大学 建筑学院,长沙 410007)

**摘 要**:自然通风能有效降低室内污染物浓度,包括稀释生物气溶胶浓度,穿堂风是其主要形式之一。但在人口稠密的城市,建筑之间的遮挡作用会明显降低通风效果。以两栋建筑为研究对象,讨

**Received**:2020-02-24

**Foundation items**: Natural Science Foundation of China (No. 51308206, 51474105); International Science and Technology Cooperation Program of China (No. 2014DFA72190)

**Author brief**: FU Linli (1995- ), main research interest: ventilation and CFD simulation, E-mail: fulinli2018@163.com.
Yin Wei (corresponding author), associate professor, PhD, E-mail: yinwei@hunst.edu.cn.

论上游建筑的9种情形，包括不同的开窗面积与位置，对下游建筑穿堂风潜力的影响。讨论一个来流方向、两栋建筑中心线在位于这个来流方向的直线上、间距为两倍建筑宽度的情形，分析基于稳态RANS模型(Reynolds-Averaged Navier-Stokes)的CFD(Computational Fluid Dynamics)模拟风压的可靠性，结果显示，部分情形CFD模拟的可靠性不高。相对于上游建筑5%与10%的孔隙率，20%的孔隙率难以通过CFD模拟出下游建筑物的风压。风洞实验数据显示，下游建筑物的穿堂风通风潜力随上游建筑物开窗面积的增加而降低，这与一般认识相反。

**关键词**：自然通风；穿堂风；建筑遮挡作用；CFD可靠性；风洞实验

**中图分类号**：TU834.1 **文献标志码**：A **文章编号**：2096-6717(2021)01-0229-14

## 1 Introduction

The architectural wind environment mainly explores the air movement between buildings and inside and outside[1], and normally uses on-site measurement, wind tunnel experiments, and computational fluid dynamics (CFD). On-site measurement is generally adopted during the preliminary stage of studies in compact urban environments[2-3], indoor air quality[4], and cross ventilation[5-6]. Compared with on-site measurement, wind tunnel experiments can provide relatively stable results, and researchers prefer this approach to explore interference effects between two buildings[7], on tall building[8-9], by backpropagation neural networks[10], to wind-induced coupled motion[11], for interference excitation mechanisms[12], to air in wakes of buildings[13], to inside and outside air[14], by surrounding buildings[15], when considering opening characteristics on a façade[16], by turbulent incoming air[17], and to velocity field and pollution dispersion[18].

In recent years, CFD has rapidly developed, and is now widely used by researchers to investigate the airflow factors inside and outside buildings, such as in the evaluation of green buildings[19], roof geometry[20-23], naturally ventilated roofs[24-25], and internal obstacles[26]. Further, the CFD setting has been considered in various models such as large eddy simulation (LES) and Reynolds-Averaged Navier-Stokes (RANS) equations of the standard $k$-$\varepsilon$ model, the re-normalisation group (RNG) $k$-$\varepsilon$ model, the realizable $k$-$\varepsilon$ model, the shear stress transport (SST) $k$-$\omega$ model, and the turbulent Reynolds stress model (RSM). These studies showed that the LES model simulation results agreed reasonably well with the experimental data by van Hooff et al.[27] and Jiang and Chen[28]. The SST k-ω model displayed the best performance among 3D steady RANS models[29-31]. Ramponi and Blocken[29] found that diffusion is an important transport mechanism that requires selecting the correct amount of physical diffusion to reduce the numerical diffusion in the cross-ventilation of buildings, and suggested using high-resolution grids and at least second-order accurate discretization schemes. Lakehal and Rodi[32] found that most RANS models had difficulties in generating the separation region on the roof, and over-predicted the recalculation region behind the building. Smal[33] found that it was impossible to reproduce the airflow of cross-ventilation by CFD in a building shielded by 8 buildings in Tominaga's wind tunnel experiment[13]. Hawendi and Gao[34] predicted through CFD that although the external boundary wall of a building reduced the ventilation airflow rate by approximately 50%, it improved wind comfort.

To date, no studies have considered the effect of the hollow characteristics of upstream buildings on downstream buildings, such as through cross ventilation, but this situation often occurs in real life. Thus, this study focuses on the hollow characteristics of the upstream building to find out

its impact on the cross ventilation potential of the downstream building, which can reduce the concentration of indoor pollutants, including that of biological aerosols. The study only investigates the distribution of upstream and downstream buildings that are not on the same straight line. As early research, it only considers two buildings, the elemental form of the building group, and the hollow characteristics in terms of elevation and window area on the upstream building.

The large eddy simulation was used in the early stage of the study, but the LES simulation time was too long, and the calculation results are unstable for 3 months. After considering the time cost and hardware conditions, it was decided to use the steady-state Reynolds average model for calculation. Our previous study discussed the reliability of 5 common RANS models: the standard $k$-$\varepsilon$ model, the re-normalisation group (RNG) $k$-$\varepsilon$ model, the realizable $k$-$\varepsilon$ model, the shear stress transport (SST) $k$-$\omega$ model, and the turbulent Reynolds stress model (RSM), for one situation (10% window in the middle) and found that the SST $k$-$\omega$ model has the highest reliability[35]. We used this model to reproduce 9 different window areas and positions for the upstream building through CFD and compare the results with experimental data in the wind tunnel to evaluate the reliability of the CFD simulation for engineering applications.

## 2 Experimental methods

### 2.1 Experimental models

The upstream and downstream building models are similar to Tominaga and Blocken[13] and Karava et al.[16] with a length scale of 1∶100. The building model dimensions are 0.2 m × 0.2 m × 0.16 m (depth × width × height), and the distance between the two buildings is fixed at 0.4 m, which is twice the building width. The study focuses on only one approaching wind direction that is perpendicular to the windward side of the upstream building. The upstream building is hollow with a couple of symmetrical openings at the windward and leeward facades. A total of nine experimental cases under different geometrical settings are summarized in Table 1, and their schematic diagram is shown in Fig. 1. Pressure taps are installed on the walls of the downstream building, as shown in Fig. 2.

**Table 1 Detailed configuration of models**

| Configuration | Opening location (elevation above ground) | | $A_1$/% (Windward window) | $A_2$/% (Leeward window) | Abbreviation (e.g. L5W=low 5% window) |
|---|---|---|---|---|---|
| | Inlet/mm | Outlet/mm | | | |
| C1 | 21 | 21 | 5 | 5 | L5W |
| C2 | 13 | 13 | 10 | 10 | L10W |
| C3 | 0 | 0 | 20 | 20 | L20W |
| C4 | 67 | 67 | 5 | 5 | M5W |
| C5 | 62 | 62 | 10 | 10 | M10W |
| C6 | 53 | 53 | 20 | 20 | M20W |
| C7 | 113 | 113 | 5 | 5 | H5W |
| C8 | 111 | 111 | 10 | 10 | H10W |
| C9 | 106 | 106 | 20 | 20 | H20W |

### 2.2 Wind tunnel settings

The experiments were carried out in the atmospheric boundary layer (ABL) wind tunnel at Hunan University of Science and Technology, which has a cross-section of 3 m × 4 m (height × width), and is 21 m in length. A combination of

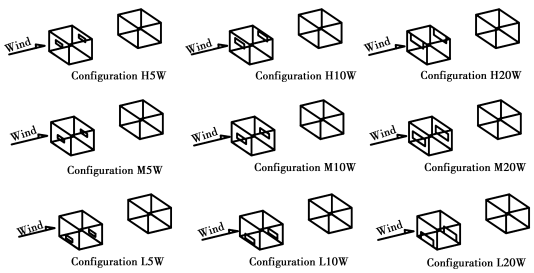


**Fig. 1 Schematic diagram of configuration**

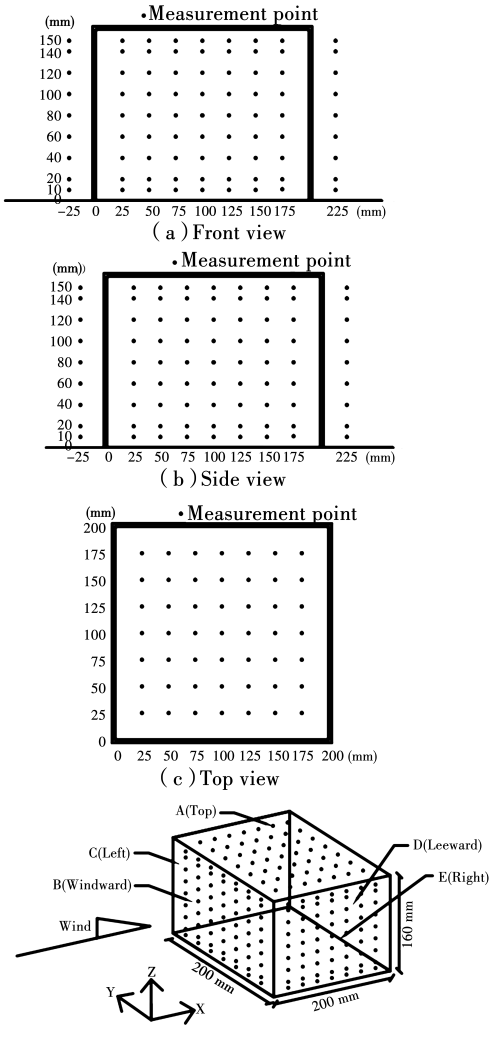


**Fig. 2 Measurement points of downstream building in**

spires and surface roughness was used to create an approach-flow wind profile representative of the lower part of an approximate ABL in the outskirts. The mean streamwise velocity of this incoming flow obeys a power law with an exponent of 0.18, as shown in Eq. (1).

$$\frac{U_Z}{U_H} = \left(\frac{z}{H}\right)^{0.18} \tag{1}$$

where $U_z$ and $U_H$ (m/s) are the mean streamwise velocity at height $z$ (m) and at the reference of building height $H$ (m), respectively.

The turbulent kinetic energy $\kappa$ is obtained using three-component measurement of the variances in the velocity fluctuations. This distribution can be approximated by using the following relation in Eq. (2).[13]

$$\frac{\kappa(z)}{U_H^2} = -0.058\exp\left(-0.19\left(\frac{z}{H}\right)\right) \tag{2}$$

where $\kappa(z)$ ($m^2/s^2$) is the turbulent kinetic energy at height $z$ (m).

Fig. 3 depicts the measured velocity curve of the incoming wind and the energy curve of the turbulent flow in the wind tunnel. The measured $U_H$ at a reference height of 0.16 m from the ground is 4.5 m/s, to yield a building Reynolds number of approximately 47 000. This Reynolds number is close to 45 000 in the experiment of Tang and Kwok.[12], Tominaga and Blocken[13], which means that the flow enters a completely turbulent state. In this state, the flow field in the atmosphere is completely similar to the flow field of a wind tunnel, so-called Renault independence.

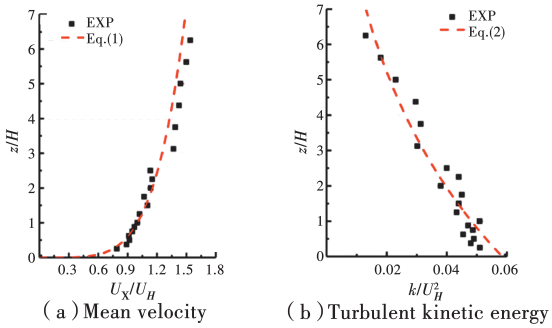


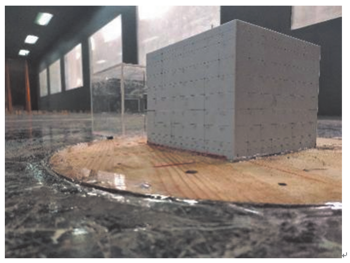

(c) Wind tunnel

**Fig. 3 Approaching flow profiles**

Experimental data acquisition included the approaching wind speed, wind pressure, static

pressure, turbulence, etc. The 3-components of velocity and local reference pressure in real-time were measured using a Cobra probe, and 301 pressure taps were tested with a frequency of 332.5 Hz within a 30-second time interval for each experiment.

## 3 CFD settings

### 3.1 Computational domain and grid

The CFD model was identical to the wind tunnel experiment model, and the thickness of the walls and ceiling was set to 3 mm. The computational domain was constructed based on the best practice guidelines in the literature [27, 29, 36], at a distance of $5H$ from the building at the top and sides of the computational domain, and $15H$ between the building and the outlet boundary downstream of the building, and 3 times the height of the building to limit the occurrence of unintended streamwise gradients in the approach flow profiles[36]. The resulting domain dimensions were 5.32 m×1.8 m×0.96 m ($L\times W\times H$), which is consistent with the computational domain illustrated by Van Hooff et al.[27]. The calculation domain size and building model grid are shown in Fig. 4, considering M10W as an example.

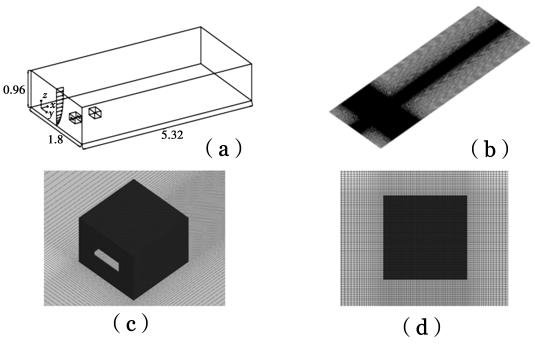


**Fig. 4 (a)Computational domain(m) (b)Grid of ground (c)Gird adjacent to upstream building (d)Top view of grid near downstream building**

### 3.2 Boundary conditions

The boundary conditions of the domain in Fluent were as follows: ground and building surfaces were defined as the wall; the top and both the sides of the calculation domain were in symmetry; the outlet is vent outflow; the inlet is velocity inlet. The velocity and turbulent energy curves were reproduced to use user-defined functions (UDF) compiled with the profiles from wind tunnel experimental data. A logarithmic inlet velocity profile was constructed based on a fit with the power-law profile as described in Eq. (3)[27].

$$U_{(Z)}=\frac{u_H^*}{\kappa}\ln\left(\frac{z+z_0}{z_0}\right) \tag{3}$$

where $u_H^*$(m/s) is the friction velocity in the wind tunnel experiment, $\kappa$ is the von Karman constant (0.42), and $z$ is the height coordinate. The logarithmic law is preferred over the power-law because it yields the value of $u_H^*$ that is required for the profile of the turbulence dissipation rate ε. The aerodynamic roughness length, $z_0$ (m), is determined based on a fitting procedure use the measured velocity profile yielding $z_0=0.000\ 9$ m at a reduced scale. Eq. (4) describes the calculation of the turbulent dissipation rate using Eq. (2)[27].

$$\varepsilon(z)=\frac{(u_H^*)^3}{\kappa(z+z_0)} \tag{4}$$

The specific dissipation rate $\omega$ for the SST $k$-$\omega$ model is calculated to use Eq. (5)[27].

$$\omega(z)=\frac{\varepsilon(z)}{C_\mu k(z)} \tag{5}$$

where $C_\mu$ is an empirical constant equal to 0.09. This part adopts the settings in Van Hooff et al.[27] and Gousseau et al.[36-37].

Using the Fluent software licensed by ANSYS for calculation, previous studies showed that the reliability and accuracy of the SST $k$-$\omega$ model simulation are the highest[29, 31, 38]. And in our last simulation of porous buildings[38], we also found that the SST model is more accurate than other RANS models. Therefore, all the cases presented here are simulated using this model. All the control equations are discretized by the second-order finite volume method, and the Semi-Implicit Method for Pressure Linked Equations (SIMPLE) algorithm is used for the pressure-velocity coupling. The computational grid was built as fully cubic structured mesh whose quality was among 0.95 and

1, the total number of grids is about 6 million. The residual of continuity and others was set as $10^{-5}$. With the Intel Xeon 32-core processor, all the models were calculated within two months.

### 3.3 Data processing method

The mean wind pressure coefficients of each point were obtained using Eq. (6) for the experimental and simulation results[25].

$$C_P = \frac{P - P_0}{\frac{1}{2}\rho U_H^2} \tag{6}$$

where $C_p$ is the mean wind pressure coefficient of each point, $P$(Pa) is the wall pressure, $P_0$(Pa) is the reference pressure, $\rho$ (kg/m$^3$) is the air density, and $U_H$(m/s) is the airflow velocity at the building height. The normalized mean wind pressure coefficients of each surface are calculated to use Eq. (7).

$$S_{C_{Pi}} = \frac{\overline{C_{Pi}}}{|\overline{C_P}|} \tag{7}$$

where $S_{C_{Pi}}$ is the normalized mean wind pressure coefficient of the $i$-face in the downstream building where $i$ represents $A$, $B$, $C$, $D$, and $E$. $\overline{C_{Pi}}$ is the surface mean wind pressure coefficient of the $i$-face in the downstream building and $|\overline{C_P}|$ is the absolute mean of the average wind pressure system at all the measuring points in the downstream building. The nine cases are L5W-0.12, L10W-0.11, L20W-0.18, M5W-0.12, M10W-0.13, M20W-0.15, H5W-0.13, H10W-0.16, H20W-0.19. $S_{C_{Pei}}$ is defined as the $i$-face normalized wind pressure coefficient of the wind tunnel experiment. The error between simulation and experiment is presented in Eq. (8) as follows

$$E = \sqrt{\frac{\sum_i^5 \left(\frac{S_{C_{Pi}}}{S_{C_{Pei}}} - 1\right)^2}{5}} \tag{8}$$

where $E$ is the error between the simulation and experimental results.

## 4 Errors analysis of CFD simulations

The viscosity model, setting method and experimental verification of CFD have been completed in paper [35] (for the 10% aperture ratio), so this paper discusses different aperture ratios and locations. The simulation reliability of nine different porous cases in the upstream is analysed. The top surface of the downstream building is defined as $A$, the windward facade as $B$, the left side along the incoming wind direction as $C$, the right side along the incoming wind direction as $E$, and the leeward facade of the downstream building as $D$. The exploded view is shown in Fig. 5. To reduce the influence of variation in the incoming wind speed, the mean pressure coefficients of the nine models are normalized. In other words, the ratio of the wind pressure coefficient of each surface to the mean wind pressure coefficients of the five faces (equal to the mean wind pressure coefficients of all the measuring points in the downstream building) is considered. Further, the CFD numerical errors compared to the experiment are listed in Table 2, where Exp1 and Exp2 are the first and second time experimental results in the wind tunnel.

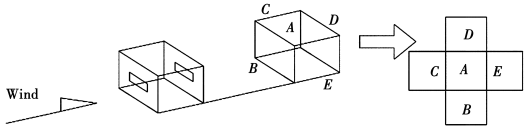


**Fig. 5 Exploded view of each surface of the downstream building: *A*-top surface; *B*-windward facade; *C*-left surface; *D*-leeward facade; *E*-right surface**

**Table 2 Standardized numerical analysis of nine different models**

%

| Configuration | L5W | L10W | L20W | M5W | M10W | M20W | H5W | H10W | H20W |
|---|---|---|---|---|---|---|---|---|---|
| Error to Exp1 | 28 | 60 | 198 | 21 | 11 | 534 | 8 | 46 | 78 |
| Error to Exp2 | 36 | 24 | 36 | 27 | 10 | 61 | 23 | 23 | 34 |
| Average error | 32 | 42 | 117 | 24 | 11 | 298 | 16 | 35 | 56 |

Each row in Table 2 shows that the reliability of the simulation results in cases using the same RANS model of SST $k$-$\omega$ is different. Under all conditions, the 10% aperture ratio in the middle of the upstream building (M10W) has the highest accuracy, with errors of 11% and 10%, when compared to Exp1 and Exp2, respectively.

In the third row, the errors of the 20% aperture ratios at low, middle, and high positions (L20W, M20W, and H20W), are an average of 117%, 298%, and 56%, respectively. It is speculated that different hole characteristics have different effects on the airflow between buildings, resulting in different airflow stability around the downstream buildings, so the simulation results using the RANS model are different.

When each error between Exp1 and Exp2 is compared, except M10W, all show obvious diversity. This indicates that the wind pressure on the model is unstable in the two sequential experiments.

Inshort, the M10W simulation reliability is the highest, with an average error of 11%, and the M20W simulation reliability is the worst, with an average error of 298%. When the building has a large opening, the airflow through the upstream building, that is, the cross ventilation, disturbs the airflow around the downstream building, resulting in a large error in the simulation results of the large opening.

In the following section, the nine different conditions are grouped into three elevations including low, middle, and upper based on the height of the upstream building window for detailed analysis.

## 5 Reliability analysis of cross ventilation potential

### 5.1 Opening at a low position

The influence of different opening sizes on the simulation reliability of the lower opening of the upstream building is considered. To analyze the pressure change at typical locations, the average wind pressure coefficient distribution on the waistline and backline of the downstream building is used to determine the difference between different occlusion situations. Fig. 6 is a schematic diagram of the middle backline and the middle waistline based on the profile of the mean coefficient of pressure ($C_p$) from the wind tunnel measurement on the downstream building surface. Fig. 7 shows $C_p$ along the middle backlines and middle waistlines on L5W, L10W, and L20W. The red dot and the black square separately denote the wind pressure coefficients in Exp1 and Exp2, respectively.

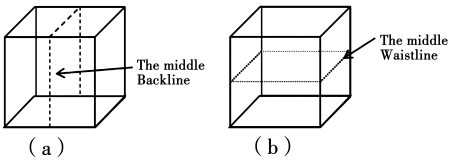


**Fig. 6 Schematic diagram of (a) Middle backine (b) Middle waistline**

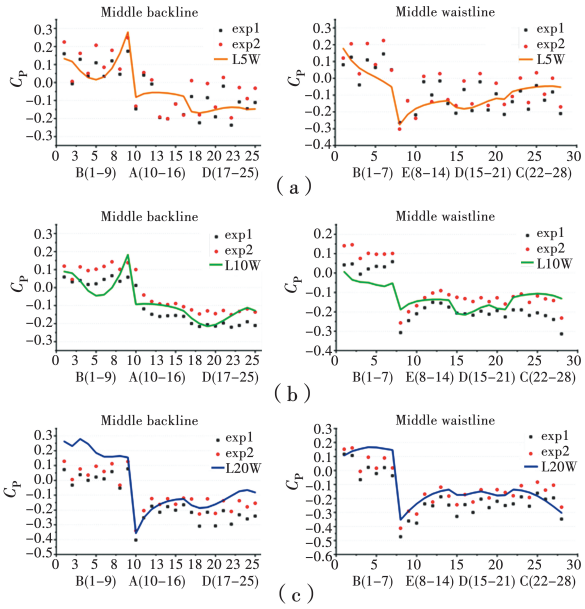


**Fig. 7 Middle backline and middle waistline of (a) L5W (b) L10W (C) L20W**

In the experiment, the pressure on the left and right sides of the downstream building may not be symmetrical due to the blockage of the upstream building and the effect of the wind. In the smoke experiment, the airflow passing through the

upstream building hit the surface of the downstream building, and unlike in the single building experiment, the airflow relatively continuously affected the building surface. However, although the surface wind pressure distributions of repeated experiments are different, they have obvious similarities. In many experiments, including experiments repeated after 3 months, the *C* facade and the *E* facade are not completely symmetrical. This is different from common sense but is actually presented by experimental and simulated data.

The simulation results among three different porosities at a low position show the following:

1) From Fig. 7(a), it is clear that when the upstream building has a small opening at a low position (L5W), the diversity of the pressure measurement in the two experiments is large. In Fig. 7(b) and (c), when the upstream building has a medium-size or large-size opening (L10W, L20W), the pressure difference between the two experiments is small.

2) In the test, compared with the other two cases, the average $C_p$ shown in Fig. 7(a) is the most unstable on these two curves.

3) Fig. 7(a) depicts the simulation results of the surface pressures of the downstream building in L5W, which are in good agreement with the experimental results.

4) Fig. 7(b) shows that in L10W, the underestimation of $C_p$ by CFD is presented on the waistline from 1 to 7 points on the windward facade *B*. However, the fitting of the other surfaces is much better.

5) In Fig. 7(c), the simulation results are overestimated in the backline (1 to 9 points on the windward facade *B*), as well as in the waistline. The overestimation of $C_p$ by CFD on the backline is more obvious than the waistline.

Fig. 8 shows the photos of a smoke effect taken in a wind tunnel, with the opening position at a low level. Fig. 9 shows the schematic diagram of the vertical middle plane and horizontal plane at a height of 0.08 m from the bottom of the ground. The diagrams of the velocity vector on these two planes are shown in Fig. 10.

(a) L5W

(b) L10W

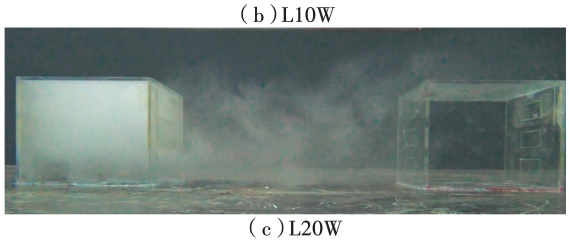

(c) L20W

**Fig. 8 Smoke visualization: windows at low position with 5%, 10%, 20% porosity**

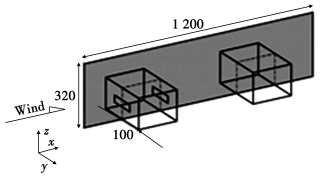


(a) Vertical middle plane

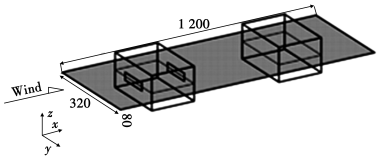


(b) Horizontal plane at a height of 0.08 m from the bottom of the ground

**Fig. 9 Schematic diagram between the two buildings**

From Fig. 8 and Fig. 10, the following can be determined:

1) As shown in Fig. 8(a) and 10(a), in the vertical velocity vector diagram, when the upstream building has a small opening at a low position (L5W), the airflow passing through the upstream building shows an upward trend at the exit.

2) In Fig. 8(b) and the vertical velocity vector

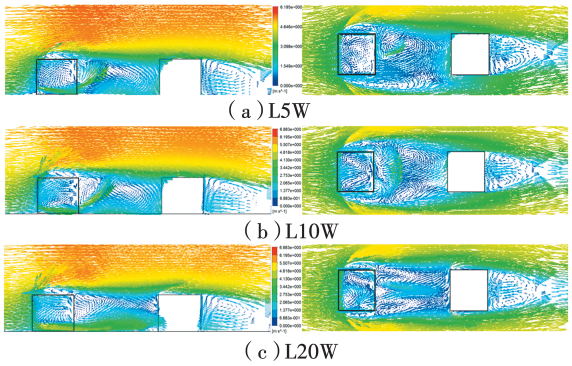


**Fig. 10 Velocity vector diagram of the vertical middle plane and the horizontal plane at a height of 0.08 m between the two buildings**

diagram in Fig. 10(b), the outflow of the cross-ventilation in the L10W case is longer than that in the L5W, and the cross-ventilation is also showing an upward trend.

3) Fig. 8(c) and Fig. 10(c) show that in L20W, the air crossing from the upstream building destroys the original airflow vortex between the buildings, and directly crashes the downstream building in a manner that is more powerful than the above-mentioned two cases. The conflict between the crossing air and return air results in the instability of the airflow. The airflow around the downstream building is unstable, and the steady-state Reynolds average model cannot reproduce such unstable fluctuations. Thus, this could be the reason for a larger CFD error when compared to the two experiments whose errors are 198% and 36%, respectively, as shown in Table 2.

In short, it is clear that when the size of the opening at a low position of the upstream building increases, the damage caused by crossing air to the return airflow between the buildings is enhanced. Further, the reliability of the simulation results is less accurate when the size of the opening increases.

### 5.2 Opening at a middle position

The effect of different aperture ratios on the simulation reliability of the middle opening of the upstream building is analysed. The $C_p$ along the middle backlines and the middle waistlines on M5W, M10W, and M20W are considered, as shown in Fig. 11, where the red dot and the black square separately indicate the wind pressure coefficients in Exp1 and Exp2, respectively. Fig. 12 shows the photos of smoke visualization taken in a wind tunnel, with the position of the opening at a middle level. The diagrams of the velocity vector on the vertical middle plane and the horizontal plane are shown in Fig. 13.

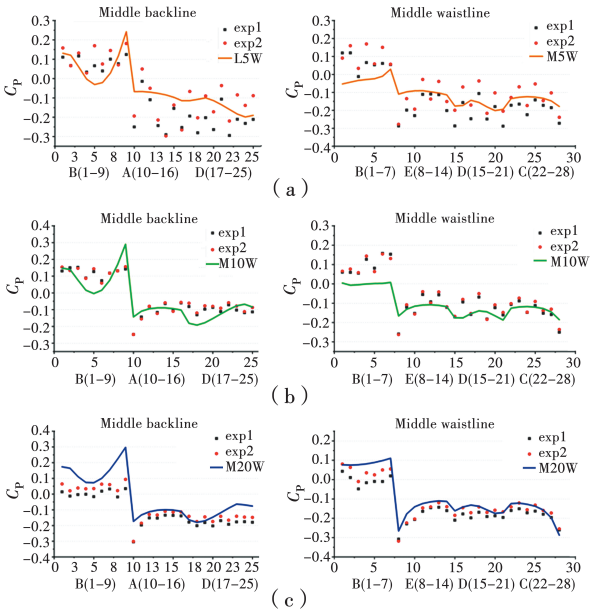


**Fig. 11 Middle backline and middle waistline of (a)M5W, (b) M10W and (c) M20W**

The main observations from Fig. 11, 12, and 13 are as follows:

1) According to Fig. 11(a), when the upstream building has a small opening (M5W), the pressure measurement diversity in the two experiments is large. This is the same as when the opening is low.

2) In Fig. 11(a) and (b), the simulation results of $C_p$ in the waistline of the windward surface (1 to 7 points on $B$) of the downstream building in the M5W and M10W configurations are lower than the wind tunnel experiment. However, the other surfaces of M10W show good fitting results. Fig. 11(c) shows that the simulation results of $C_p$ are overestimated on all surfaces of the downstream building in the M20W configuration, the backline and waistline of windward of the

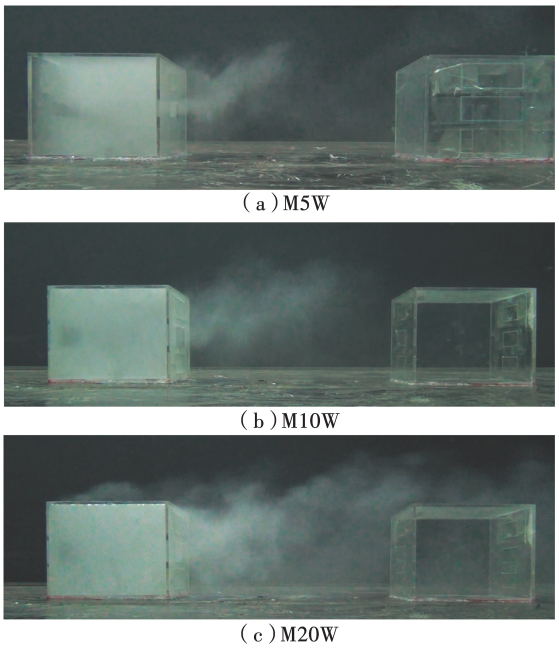

(a) M5W

(b) M10W

(c) M20W

**Fig. 12 Smoke visualization: windows at middle position with 5%, 10%, 20% porosity**

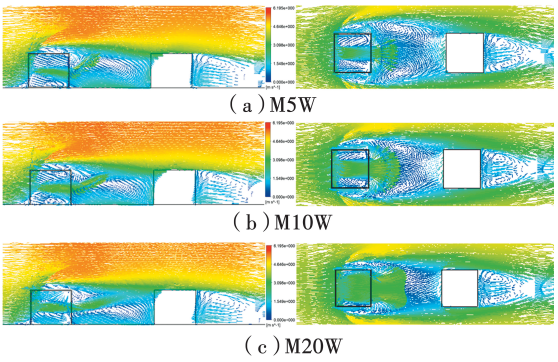

(a) M5W

(b) M10W

(c) M20W

**Fig. 13 Velocity vector diagram of the vertical middle plane and the horizontal plane at a height of 0.08 m between the two buildings**

downstream building being the most noticeable.

3) From smoke visualization in Fig. 12 and the velocity vector diagram depicted in Fig. 13 (a), (b), and (c), it is seen that as the opening rate at the middle position increases, the outflow distance of cross-air increases, and the damage to the original airflow between the buildings enhances. Compared to the L20W configuration, the vortex is destroyed when the opening is at the middle position, but the original airflow between the buildings is not destroyed. This could be why the simulations of M5W and M10W are more reliable when their errors are 24 % and 11 %, respectively, as shown in Table 2.

Inshort, when the size of the opening at the middle position of the upstream building increases, the damage caused by crossing air to the return airflow between the buildings also increases. However, the reliability of the simulation results does not decrease with an increase in the aperture ratio, and the accuracy of the M10W simulation is the greatest. This is different from the discussion in section 5.1.

### 5.3 Opening at a high position

Fig. 14(a), (b), and (c) show the schematic diagrams of the mean wind pressure coefficient of the middle backline and the middle waistline on H5W, H10W, and H20W, respectively. Fig. 15 shows the photos of smoking effect with the window position at a high level. Fig. 16 shows the simulation results of velocity vector of the vertical middle plane and the horizontal plane at a height of 0.08 m from the ground between the buildings.

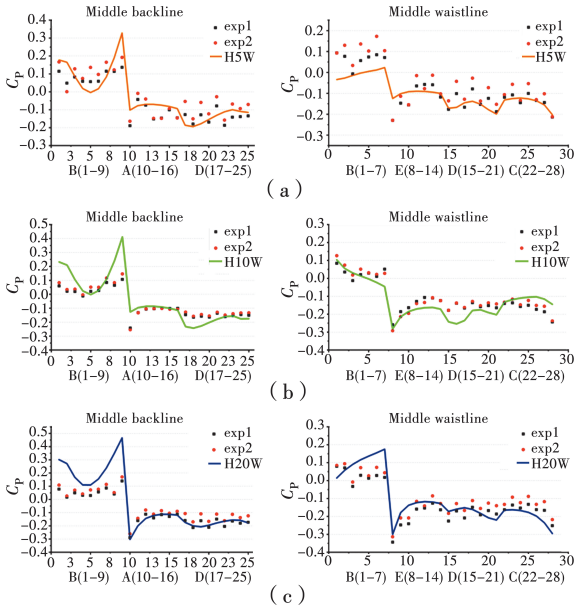


**Fig. 14 Middle backline and middle waistline of (a) H5W (b) H10W (c) H20W**

The most important observations from Fig. 14, 15, and 16 are as follows:

1) As seen in Fig. 14(a), when the upstream building has a small sized opening at a high position (H5W), the pressure measurement diversity in the two experiments is large. Fig. 8, 11, and 14 show

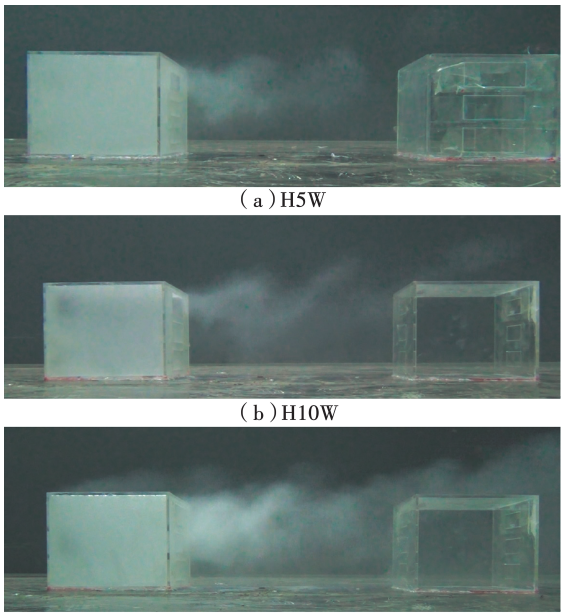

(a) H5W

(b) H10W

(c) H20W

**Fig. 15 Smoke visualization: windows at high position with 5%, 10%, 20% porosity**

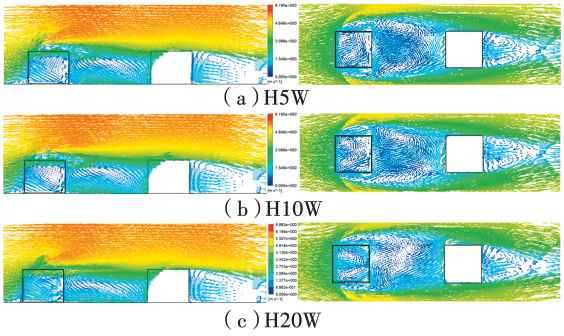

(a) H5W

(b) H10W

(c) H20W

**Fig. 16 Velocity vector diagram of the vertical middle plane and the horizontal plane at a height of 0.08 m between the two buildings**

that when the ratio of the opening of the upstream building is not less than 10%, the surface pressure fluctuation of the downstream building is small.

2) As seen in Fig. 14(a), in the configuration of H5W, the simulation results of $C_p$ on the windward surface of the waistline (1 to 7 points on facade $B$) on the downstream building are underestimated compared to the experimental results. However, the fitting results of the H10W configuration on all the surfaces are much better, as shown in Fig. 14(b). Fig. 14(c) shows that the simulation results of $C_p$ of M20W are overestimated on the backline (1 to 9 points on facade $B$) on the windward surface, as well as on the waistline (1 to 7 points on facade $B$).

3) The smoking photos in Fig. 15 and velocity vector diagrams in Fig. 16(a), (b), and (c) show that when a window is at a high position, the change in the size of the opening rarely influences the vortex between the two buildings. Consequently, the simulation results of openings at a high position of the upstream building are better than openings at a low position. The average error of H10W is 35% compared with 42% of L10W, and the average error of H20W is 56% compared to 117% of L20W.

In short, when the opening is at a high position of the upstream building, different opening ratios of the upstream building have less effect on the airflow between the buildings, and the simulation reliability decreases as the aperture ratios increase.

### 5.4 Cross ventilation potential

As the reliability of CFD simulation in such problems is not high, the subsequent analysis is based on experimental data. The potential for cross ventilation is determined by the pressure difference between the windward and leeward facades of the building. The experimental values are shown in Table 3.

**Table 3 Coefficient of pressure difference ($\Delta P$) between the windward and leeward in experiment**

| Position | $C_p$ | 5% | 10% | 20% |
|---|---|---|---|---|
| High | $C_{p\text{-windward}}$ | 0.14 | 0.06 | 0.05 |
| | $C_{p\text{-leeward}}$ | −0.17 | −0.17 | −0.17 |
| | $\Delta P_{exp}$ | ***0.31*** | ***0.23*** | ***0.22*** |
| Middle | $C_{p\text{-windward}}$ | 0.09 | 0.08 | 0.01 |
| | $C_{p\text{-leeward}}$ | −0.20 | −0.18 | −0.19 |
| | $\Delta P_{exp}$ | ***0.29*** | ***0.26*** | ***0.20*** |
| Low | $C_{p\text{-windward}}$ | 0.13 | 0.05 | 0.03 |
| | $C_{p\text{-leeward}}$ | −0.17 | −0.19 | −0.20 |
| | $\Delta P_{exp}$ | ***0.30*** | ***0.24*** | ***0.23*** |

The most important observations from Table 3 are as follows:

1) Along with the increase in the opening area, the pressure difference gradually decreases.

The pressure difference of 20% opening rate is reduced by 30% in comparison to 5%, which is the exact opposite of our feeling that the larger the opening, the greater the amount of ventilation. It was observed in the experiment that the crossing airflow filled the return area between the two buildings, and at the same time crowded out the bypass airflow that would hit the windward facade of the downstream building.

2) In all cases, the average wind pressure on the leeward side is almost constant, while the pressure on the windward side changes significantly. This shows that the change in the pressure difference before and after the building is caused by the pressure change on the windward side. This is consistent with the above analysis.

3) The change of the opening height-high, middle and low-has no obvious effect on the pressure difference.

In short, the pressure difference between the front and rear of the downstream building decreases with the increase of the opening area of the upstream building, and has little relationship with the opening position.

## 6 Conclusions

Based on a strict comparison with the wind tunnel experiment, this paper analyses the reliability and accuracy of CFD simulation of surface pressure of downstream building under different opening conditions of upstream buildings. The following conclusions have been obtained:

1) The data of multiple experiments show that the wind pressure distribution on the surface of the blocked block is not strictly symmetrical, for example, the $C$ facade and the $E$ facade are not completely the same. Moreover, in repeated experiments, the pressure distribution cannot be completely reproduced. These are different from general beliefs, but they were indeed observed in our experiments. Smoke experiments showed that the air flow behind the upstream building was flapping on the downstream building. However, in general, the wind pressure distribution on the surface of the downstream building was similar during the decompression experiment.

2) The standardized values of nine configurations showed that the reliability varied for the different configurations. The highest reliability was observed for M10W with an average error of 11%, and the worst accuracy was observed for M20W with an average error of 298%.

3) The analysis of $C_p$ on the middle backline and middle waistline of the cube showed that when the upstream building had a small opening, such as L5W, M5W, and H5W, the repeated experiments of pressure measurement varied drastically. When the upstream building has an opening ratio of 20%, the airflow passing through the upstream building, that is, the wind passing through the upstream building, has a greater impact on the original airflow vortex between the two buildings, which leads to unstable airflow around the downstream building. RANS model seems difficult to reproduce this phenomenon.

4) When the opening was at a low or high position, the reliability of the CFD simulation decreased with an increase in the opening rate.

5) In the velocity vector diagram, conflictis seen between the crossing air and return air between buildings that changed with different aperture ratios when there was an opening in the middle or lower part of the building. However, when the window was opened at the upper part of the facade, the change of the size of the opening showed a rare influence on the vortex between the two buildings.

6) The cross ventilation potential of the downstream building decreases with the increase of the size of the opening of the upstream building and has little relationship with the opening position, which is contrary to general beliefs.

The limitations of this study are also obvious. This study has focused only on one wind direction, one spacing, and one steady-state RANS model of SST $k$-$\omega$. The LES model needs to be considered inthe future. And the paper only discusses the distribution of the center lines of the upstream and downstream buildings that are not on the same straight line. This study also found that when the

building opening is located at the bottom, the accuracy of the CFD prediction decreases and the cause of the decrease in prediction accuracy will also be analyzed in subsequent studies. In addition, the architectural model adopted in this article has certain specificity, and the follow-up research can be further studied for general architecture.

## Acknowledgements

The authors would like to acknowledge the financial support from the National Natural Science Foundation of China (Grant No. 51308206, 51474105) and the International Science and Technology Cooperation Program of China (No. 2014DFA72190).

References:

[1] YIN W, ZHANG G Q, YANG W, et al. Natural ventilation potential model considering solution multiplicity, window opening percentage, air velocity and humidity in China [J]. Building and Environment, 2010, 45(2): 338-344.

[2] TABLADA A, DE TROYER F, BLOCKEN B, et al. On natural ventilation and thermal comfort in compact urban environments-the Old Havana case [J]. Building and Environment, 2009, 44(9): 1943-1958.

[3] KHANDURI A C, STATHOPOULOS T, BÉDARD C. Wind-induced interference effects on buildings: A review of the state-of-the-art [J]. Engineering Structures, 1998, 20(7): 617-630.

[4] HESARAKI A, MYHREN J A, HOLMBERG S. Influence of different ventilation levels on indoor air quality and energy savings: A case study of a single-family house [J]. Sustainable Cities and Society, 2015, 19: 165-172.

[5] MOCHIDA A, YOSHINO H, TAKEDA T, et al. Methods for controlling airflow in and around a building under cross-ventilation to improve indoor thermal comfort [J]. Journal of Wind Engineering and Industrial Aerodynamics, 2005, 93(6): 437-449.

[6] CONCEIÇÃO E Z E, LÚCIO M J R, VICENTE V D S R, et al. Evaluation of local thermal discomfort in a classroom equipped with cross flow ventilation [J]. International Journal of Ventilation, 2008, 7(3): 267-277.

[7] KIM W, TAMURA Y, YOSHIDA A. Interference effects on aerodynamic wind forces between two buildings [J]. Journal of Wind Engineering and Industrial Aerodynamics, 2015, 147: 186-201.

[8] TANIIKE Y, INAOKA H. Aeroelastic behavior of tall buildings in wakes [J]. Journal of Wind Engineering and Industrial Aerodynamics, 1988, 28(1/2/3): 317-327.

[9] TANIIKE Y. Turbulence effect on mutual interference of tall buildings [J]. Journal of Engineering Mechanics, 1991, 117(3): 443-456.

[10] KHANDURI A C, BÉDARD C, STATHOPOULOS T. Modelling wind-induced interference effects using backpropagation neural networks [J]. Journal of Wind Engineering and Industrial Aerodynamics, 1997, 72: 71-79.

[11] THEPMONGKORN S, WOOD G S, KWOK K C S. Interference effects on wind-induced coupled motion of a tall building [J]. Journal of Wind Engineering and Industrial Aerodynamics, 2002, 90(12-15): 1807-1815.

[12] TANG U F, KWOK K C S. Interference excitation mechanisms on a 3D of aeroelastic CAARC building model [J]. Journal of Wind Engineering and Industrial Aerodynamics, 2004, 92(14/15): 1299-1314.

[13] TOMINAGA Y, BLOCKEN B. Wind tunnel experiments on cross-ventilation flow of a generic building with contaminant dispersion in unsheltered and sheltered conditions [J]. Building and Environment, 2015, 92: 452-461.

[14] OHBA M, IRIE K, KURABUCHI T. Study on airflow characteristics inside and outside a cross-ventilation model, and ventilation flow rates using wind tunnel experiments [J]. Journal of Wind Engineering and Industrial Aerodynamics, 2001, 89(14/15): 1513-1524.

[15] SHIRZADI M, TOMINAGA Y, MIRZAEI P A. Wind tunnel experiments on cross-ventilation flow of a generic sheltered building in urban areas [J]. Building and Environment, 2019, 158: 60-72.

[16] KARAVA P, STATHOPOULOS T, ATHIENITIS A K. Airflow assessment in cross-ventilated buildings with operable façade elements [J]. Building and Environment, 2011, 46(1): 266-279.

[17] ETHERIDGE D W, NOLAN J A. Ventilation measurements at model scale in a turbulent flow [J]. Building and Environment, 1979, 14(1): 53-64.

[18] TOMINAGA Y, BLOCKEN B. Wind tunnel analysis of flow and dispersion in cross-ventilated isolated buildings: Impact of opening positions [J]. Journal of Wind Engineering and Industrial Aerodynamics, 2016, 155: 74-88.

[19] GUO W H, LIU X, YUAN X. Study on natural

ventilation design optimization based on CFD simulation for green buildings [J]. Procedia Engineering, 2015, 121: 573-581.

[20] PERÉN J I, VAN HOOFF T, LEITE B C C, et al. CFD analysis of cross-ventilation of a generic isolated building with asymmetric opening positions: Impact of roof angle and opening location [J]. Building and Environment, 2015, 85: 263-276.

[21] PERÉN J I, VAN HOOFF T, LEITE B C C, et al. CFD simulation of wind-driven upward cross ventilation and its enhancement in long buildings: Impact of single-span versus double-span leeward sawtooth roof and opening ratio [J]. Building and Environment, 2016, 96: 142-156.

[22] PERÉN J I, VAN HOOFF T, LEITE B C C, et al. Impact of eaves on cross-ventilation of a generic isolated leeward sawtooth roof building: Windward eaves, leeward eaves and eaves inclination [J]. Building and Environment, 2015, 92: 578-590.

[23] PEREN J I, VAN HOOFF T, RAMPONI R, et al. Impact of roof geometry of an isolated leeward sawtooth roof building on cross-ventilation: Straight, concave, hybrid or convex? [J]. Journal of Wind Engineering and Industrial Aerodynamics, 2015, 145: 102-114.

[24] LI D, ZHENG Y M, LIU C Y, et al. Numerical analysis on thermal performance of naturally ventilated roofs with different influencing parameters [J]. Sustainable Cities and Society, 2016, 22: 86-93.

[25] CHU C R, CHIU Y H, CHEN Y J, et al. Turbulence effects on the discharge coefficient and mean flow rate of wind-driven cross-ventilation [J]. Building and Environment, 2009, 44(10): 2064-2072.

[26] CHU C R, CHIANG B F. Wind-driven cross ventilation with internal obstacles [J]. Energy and Buildings, 2013, 67: 201-209.

[27] VAN HOOFF T, BLOCKEN B, TOMINAGA Y. On the accuracy of CFD simulations of cross-ventilation flows for a generic isolated building: Comparison of RANS, LES and experiments [J]. Building and Environment, 2017, 114: 148-165.

[28] JIANG Y, CHEN Q Y. Effect of fluctuating wind direction on cross natural ventilation in buildings from large eddy simulation [J]. Building and Environment, 2002, 37(4): 379-386.

[29] RAMPONI R, BLOCKEN B. CFD simulation of cross-ventilation for a generic isolated building: Impact of computational parameters [J]. Building and Environment, 2012, 53: 34-48.

[30] HU C H, KURABUCHI T, OHBA1 M. Numerical study of cross-ventilation using two-equation RANS [J]. International Journal of Ventilation, 2005, 4(2): 123-131.

[31] RAMPONI R, BLOCKEN B. CFD simulation of cross-ventilation flow for different isolated building configurations: Validation with wind tunnel measurements and analysis of physical and numerical diffusion effects [J]. Journal of Wind Engineering and Industrial Aerodynamics, 2012, 104/105/106: 408-418.

[32] LAKEHAL D, RODI W. Calculation of the flow past a surface-mounted cube with two-layer turbulence models [J]. Journal of Wind Engineering and Industrial Aerodynamics, 1997, 67/68: 65-78.

[33] SMAL R. CFD analysis of natural ventilation in a generic environment impact of street width on indoor airflow pattern and airflow rate [D]. Eindhoven, Netherlands: Eindhoven University of Technology, 2017.

[34] HAWENDI S, GAO S A. Impact of an external boundary wall on indoor flow field and natural cross-ventilation in an isolated family house using numerical simulations [J]. Journal of Building Engineering, 2017, 10: 109-123.

[35] FU L L, YIN W, WANG T W, et al. Reliability of CFD simulation for the wind pressure on a cubic after another cavity in comparison of wind tunnel experiment [J]. Journal of Civil and Environmental Engineering, 2020, 42(1):180-190.

[36] GOUSSEAU P, BLOCKEN B, STATHOPOULOS T, et al. CFD simulation of near-field pollutant dispersion on a high-resolution grid: A case study by LES and RANS for a building group in downtown Montreal [J]. Atmospheric Environment, 2011, 45(2): 428-438.

[37] GOUSSEAU P, BLOCKEN B, VAN HEIJST G J F. CFD simulation of pollutant dispersion around isolated buildings: On the role of convective and turbulent mass fluxes in the prediction accuracy [J]. Journal of Hazardous Materials, 2011, 194: 422-434.

[38] KURABUCHI T, OHBA M, ENDO T, et al. Local dynamic similarity model of cross-ventilation part 1-theoretical framework [J]. International Journal of Ventilation, 2004, 2(4): 371-382.

(编辑 胡英奎)